JACS
JOURNAL OF THE AMERICAN CHEMICAL SOCIETY

Article

Facile Dehydrogenation of Ethane on the IrO(110) Surface

Yingxue Bian, Minkyu Kim, Tao Li, Aravind Asthagiri, and Jason F. Weaver

J. Am. Chem. Soc., **Just Accepted Manuscript** • DOI: 10.1021/jacs.7b13599 • Publication Date (Web): 27 Jan 2018

Just Accepted

ACS Publications

Journal of the American Chemical Society is published by the American Chemical Society. 1155 Sixteenth Street N.W., Washington, DC 20036

Facile Dehydrogenation of Ethane on the $IrO_2(110)$ Surface

Yingxue Bian[1,†], Minkyu Kim[2,†], Tao Li[1], Aravind Asthagiri[2], Jason F. Weaver[1]*

[1]Department of Chemical Engineering, University of Florida, Gainesville, FL 32611, USA

[2]William G. Lowrie Chemical & Biomolecular Engineering, The Ohio State University, Columbus, OH 43210, USA

[†] Yingxue Bian and Minkyu Kim contributed equally to this work.

*To whom correspondence should be addressed, weaver@che.ufl.edu

Tel. 352-392-0869, Fax. 352-392-9513

Abstract

Realizing the efficient and selective conversion of ethane to ethylene is important for improving the utilization of hydrocarbon resources, yet remains a major challenge in catalysis. Herein, ethane dehydrogenation on the $IrO_2(110)$ surface is investigated using temperature programmed reaction spectroscopy (TPRS) and density functional theory (DFT) calculations. The results show that ethane forms strongly-bound σ-complexes on $IrO_2(110)$ and that a large fraction of the complexes undergo C-H bond cleavage during TPRS at temperatures below 200 K. Continued heating causes as much as 40% of the dissociated ethane to dehydrogenate and desorb as ethylene near 350 K, with the remainder oxidizing to CO_x species. Both TPRS and DFT show that ethylene desorption is the rate-controlling step in the conversion of ethane to ethylene on $IrO_2(110)$ during TPRS. Partial hydrogenation of the $IrO_2(110)$ surface is found to enhance ethylene production from ethane while suppressing oxidation to CO_x species. DFT predicts that hydrogenation of reactive oxygen atoms of the $IrO_2(110)$ surface effectively deactivates these sites as H-atom acceptors, and causes ethylene desorption to become favored over further dehydrogenation and oxidation of ethane-derived species. The study reveals that $IrO_2(110)$ exhibits an exceptional ability to promote ethane dehydrogenation to ethylene near room temperature, and provides molecular-level insights for understanding how surface properties influence selectivity toward ethylene production.

Introduction

Developing catalysts that can directly convert ethane to ethylene is gaining increasing interest due to the availability of light alkanes from shale gas as well as the increasing demand for ethylene. The oxidative dehydrogenation (ODH) of ethane offers advantages over non-oxidative processes and has been widely studied.[1-3] The ODH of ethane occurs in the presence of oxygen and involves the dehydrogenation of ethane to ethylene with concurrent oxidation of the released hydrogen to water. The latter step makes the ODH of ethane an exothermic process for which high conversion is thermodynamically favored at low temperature. Furthermore, the presence of oxygen in the reactant stream minimizes catalyst deactivation by coking which can be a significant problem in non-oxidative routes for ethane dehydrogenation. Various metal oxides as well as alkali chlorides are effective in promoting the ODH of ethane and propane, with VO_x-based catalysts generally exhibiting the most favorable performance.[1-9] However, the catalysts that have been investigated to date do not achieve sufficient activity and selectivity to be utilized at the industrial scale.

Initial C-H bond cleavage is widely accepted as the rate-controlling step in the ODH of ethane, and more generally in the catalytic processing of light alkanes.[1] This situation presents a challenge in developing catalysts that can selectively dehydrogenate ethane to ethylene because the reaction steps that follow initial C-H bond cleavage occur rapidly and can be difficult to control, particularly in the presence of oxygen. Recently, we have reported that CH_4 undergoes highly facile C-H bond activation on the $IrO_2(110)$ surface at temperatures as low as 150 K.[10] We find that methane adsorbs as a strongly-bound σ-complex on $IrO_2(110)$ and that C-H bond cleavage occurs by a heterolytic pathway wherein the adsorbed complex transfers a H-atom to a

lattice oxygen atom, thus affording adsorbed CH_3 and OH groups. Our results further show that the resulting methyl groups react with the $IrO_2(110)$ surface via oxidation to CO_x and H_2O as well as recombination with adsorbed hydrogen to regenerate CH_4, with these products desorbing at temperatures above ~400 K during temperature programmed reaction spectroscopy (TPRS) experiments.[10] Key findings are that the initial C-H bond cleavage of CH_4 is highly facile and that subsequent reaction steps control the overall chemical transformations of methane on the $IrO_2(110)$ surface. The ability of $IrO_2(110)$ to activate alkane C-H bonds at low temperature may provide opportunities to develop catalysts that are capable of directly and efficiently transforming light alkanes to value-added products.

In the present study, we investigated the dehydrogenation of ethane on the $IrO_2(110)$ surface. We find that initial C-H bond cleavage of C_2H_6 occurs efficiently on $IrO_2(110)$ at low temperature (~150 to 200 K) and that subsequent reaction produces C_2H_4 as well as CO_x species during TPRS, with the C_2H_4 product desorbing between 300 and 450 K. We demonstrate that partially hydrogenating the $IrO_2(110)$ surface to convert a fraction of the surface O-atoms to OH groups enhances the conversion of C_2H_6 to C_2H_4 while suppressing extensive oxidation to CO_x species. Our findings show that the controlled deactivation of surface O-atoms is an effective means for promoting the selective conversion of ethane to ethylene on $IrO_2(110)$ at low temperature.

Experimental Details

Details of the ultrahigh vacuum (UHV) analysis chamber with an isolatable ambient-pressure reaction cell utilized in the present study have been reported previously.[10] Briefly, the Ir(100) crystal employed in this study is a circular disk (9 mm × 1 mm) that is attached to a liquid-

nitrogen-cooled, copper sample holder by 0.015" W wires that are secured to the edge of crystal. A type K thermocouple was spot welded to the backside of the crystal for temperature measurements. Resistive heating, controlled using a PID controller that varies the output of a programmable DC power supply, supports linearly ramping from 80 to 1500 K and maintaining the sample temperature. Sample cleaning consisted of cycles of Ar^+ sputtering (2000 eV, 1.5 μA) at 1000 K, followed by annealing at 1500 K for several minutes. The sample was subsequently exposed to 5×10^{-7} Torr of O_2 at 900 K for several minutes to remove surface carbon, followed by flashing to 1500 K to remove final traces of oxygen.

We generated an $IrO_2(110)$ film by exposing Ir(100) to 5 Torr of O_2 (Airgas, 99.999%) for a duration of 10 minutes (3×10^9 Langmuir) in the ambient-pressure reaction cell at a surface temperature of 765 K. Our ambient-pressure reaction cell is designed to reach elevated gas pressure while maintaining UHV in the analysis chamber.[10] After preparation of the oxide film, we lowered the surface temperature to 600 K, and then evacuated O_2 from the reaction cell and transferred the sample back to the UHV analysis chamber. We exposed the film to ~23 L O_2 while cycling the surface temperature between 300 and 650 K to fill oxygen vacancies that may be created during sample transfer from the reaction cell to the analysis chamber. This procedure produces a high-quality $IrO_2(110)$ surface that has a stoichiometric surface termination, contains ~40 ML of oxygen atoms and is about 3.2 nm thick.[10,11]

The stoichiometric $IrO_2(110)$ surface consists of parallel rows of fivefold coordinated Ir atoms and so-called bridging O atoms (see Supporting Information (SI)), each of which lacks a bonding partner relative to the bulk and is thus coordinatively unsaturated (cus). Hereafter, we refer to the fivefold coordinated Ir atoms as Ir_{cus} atoms and the bridging O-atoms as O_{br} atoms. On the basis of the $IrO_2(110)$ unit cell, the areal density of Ir_{cus} atoms and O_{br} atoms is equal to

37% of the Ir(100) surface atom density of 1.36×10^{15} cm^{-2}. Since Ir_{cus} atoms are active adsorption sites, we define 1 ML as equal to the density of Ir_{cus} atoms on the $IrO_2(110)$ surface.

We studied the adsorption of C_2H_6 (Matheson, 99.999%) on clean and hydrogen pre-covered $IrO_2(110)$ using TPRS. We delivered ethane to the sample from a calibrated beam doser at an incident flux of approximately 0.0064 ML/s with the sample-to-doser distance set to about 15 mm to ensure uniform impingement of ethane across the sample surface. We prepared hydrogen pre-covered $IrO_2(110)$ by exposing the surface to varying quantities of H_2 at 90 K, followed by heating to 380 K. We have recently reported that this procedure enhances the concentration of HO_{br} groups by promoting the hopping of H-atoms on Ir_{cus} sites to O_{br}.[11] We estimate that ~0.075 to 0.15 ML of H_2 adsorbs from the vacuum background during cooling of the initially clean $IrO_2(110)$ surface, prior to a TPRS experiment. We collected TPRS spectra after ethane exposures by positioning the sample in front of a shielded mass spectrometer at a distance of about 5 mm and then heating at a constant rate of 1 K/s until the sample temperature reached 800 K. To ensure consistency in the composition and structure of the $IrO_2(110)$ layer, the surface was exposed to 23.3 L of O_2 supplied through a tube doser while cycling the surface temperature between 300 and 650 K after each TPRS experiment. Initially, we monitored a wide range of desorbing species to identify the main products that are generated from reactions of ethane on $IrO_2(110)$, and found that the only desorbing species are C_2H_6, CO, CO_2, C_2H_4, CH_4 and H_2O. We quantified desorption yields using established procedures as described in the SI.

Computational Details

All plane wave DFT calculations were performed using the projector augmented wave pseudopotentials[12] provided in the Vienna ab initio simulation package (VASP).[13,14] The Perdew-Burke-Ernzerhof (PBE) exchange-correlation functional[15] was used with a plane wave expansion cutoff of 450 eV. Dispersion interactions are modeled using the DFT-D3 method developed by Grimme et al.[16] We find that this method provides accurate estimates of the adsorption energies of n-alkanes on PdO(101)[17] and RuO_2(110)[18] in comparison with TPD-derived values; however, the DFT-D3 calculations overestimate the adsorption energy of methane on IrO_2(110).[10] We find that DFT-D3 calculations using the PBE functional also overestimate the binding energies of C_2H_4 and C_2H_6 on IrO_2(110). We compare the results of DFT-PBE calculations performed with and without dispersion corrections in the SI (Table S1), and note that the predictions from both methods support the conclusions of this study. We employed four layers to model the IrO_2(110) film, resulting in an ~12 Å thick slab with an additional 25 Å vacuum to avoid spurious interactions normal to the surface. The PBE bulk lattice constant of IrO_2 (a = 4.54 Å and c = 3.19 Å) is used to fix the lateral dimensions of the slab. The bottom two layers are fixed, but all other lattice atoms are allowed to relax during the calculations until the forces are less than 0.05 eV/Å. A 2×4 unit cell with a corresponding $2 \times 2 \times 1$ Monkhorst-Pack k-point mesh is used. In the present study, we define the binding energy, E_b, of an adsorbed C_2H_6 molecule on the surface using the expression,

$$E_b = \left(E_{C_2H_6} + E_{surf}\right) - E_{C_2H_6/surf}$$

where $E_{C_2H_6/surf}$ is the energy of the state containing the adsorbed C_2H_6 molecule, E_{surf} is the energy of the bare surface, and $E_{C_2H_6}$ is the energy of an isolated C_2H_6 molecule in the gas phase. All reported binding energies are corrected for zero-point vibrational energy. From the equation above, a large positive value for the binding energy indicates a high stability of the adsorbed C_2H_6 molecule under consideration. We evaluated the barriers for C_2H_6 dehydrogenation on the $IrO_2(110)$ surface using the climbing nudged elastic band (cNEB) method.[19] Our DFT calculations were performed for a single C_2H_6 molecule adsorbed within the 2×4 surface model of $IrO_2(110)$, and corresponds to an C_2H_6 coverage equal to 12.5% of the total density of Ir_{cus} atoms and 25% of the Ir_{cus} density within one Ir_{cus} row.

Results and Discussion

TPRS of C_2H_6 adsorbed on $IrO_2(110)$

Our TPRS results show that the $IrO_2(110)$ surface is highly reactive toward ethane as more than 90% of the C_2H_6 adsorbed on $IrO_2(110)$ oxidizes to CO, CO_2 and H_2O during TPRS at low initial C_2H_6 coverages (Figure 1a). The CO_2 and CO products desorb in TPRS peaks centered at 525 and 550 K, while H_2O desorbs over a broader feature spanning temperatures from ~400 to 750 K. We also observe a small C_2H_6 TPRS peak at 110 K that arises from weakly-bound, molecularly-adsorbed C_2H_6, likely associated with a minority surface phase.

At high initial C_2H_6 coverages, a fraction of the adsorbed C_2H_6 dehydrogenates to produce C_2H_4 in addition to undergoing extensive oxidation to CO and CO_2 (Figure 1b). Ethylene desorption accounts for about 38% of the total amount of C_2H_6 that reacts during TPRS at saturation of the initial C_2H_6 layer. The C_2H_4 TPRS feature resulting from C_2H_6 dehydrogenation on $IrO_2(110)$ exhibits a maximum at 350 K and a shoulder centered at ~425 K, and most of the

C_2H_4 desorbs at lower temperature than the CO and CO_2 products. Assuming maximum values of the desorption pre-factors (5.6×10^{18}, 1.1×10^{19} s^{-1}), we estimate that the C_2H_4 peak temperatures of 350 and 425 K correspond to C_2H_4 binding energies of 132 and 162 kJ/mol, respectively. Prior studies show that maximum desorption pre-factors are appropriate for describing the desorption of small hydrocarbons from $TiO_2(110)$ and $RuO_2(110)$ surfaces,[18,20] where the pre-factors are computed using a model based on transition state theory.[21] We have performed TPRS experiments following C_2H_4 adsorption on $IrO_2(110)$, and find that C_2H_4 desorbs in a broad feature spanning temperatures from ~150 to 500 K (see SI). The breadth of this TPRS feature likely reflects a sensitivity of the C_2H_4 binding energy and configuration(s) to the local environment, and will be addressed in a future study. Because the C_2H_4 TPRS feature resulting from C_2H_6 dehydrogenation desorbs over a similar temperature range as C_2H_4 adsorbed on $IrO_2(110)$, we conclude that C_2H_4 production from C_2H_6 on $IrO_2(110)$ is a desorption-limited process.

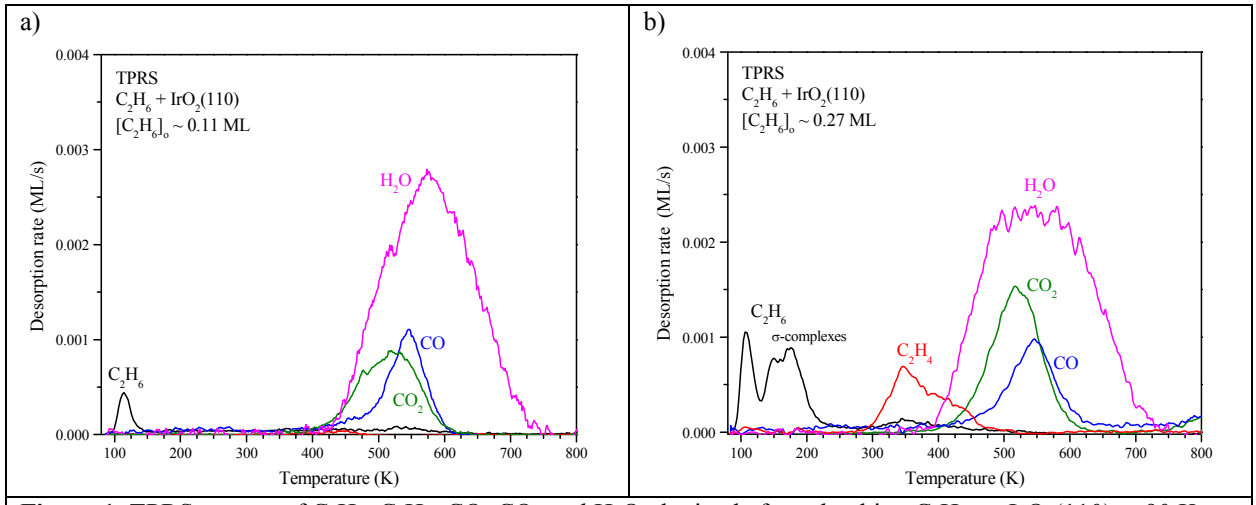

Figure 1: TPRS spectra of C_2H_6, C_2H_4, CO, CO_2 and H_2O obtained after adsorbing C_2H_6 on $IrO_2(110)$ at 90 K to reach initial C_2H_6 coverages of a) 0.11 ML and b) 0.27 ML.

A new C_2H_6 TPRS feature centered at 185 K emerges after the TPRS features generated by the CO, CO_2, C_2H_4, H_2O products first saturate at a total C_2H_6 coverage near 0.20 ML (SI), with this TPRS feature developing two maxima at ~150 and 175 K as its desorption yield begins to saturate (Figure 1b). The C_2H_6 TPRS peak at 110 K grows only slowly as the total C_2H_6 coverage increases to about 0.35 ML, but a separate peak at 120 K intensifies sharply thereafter (see Fig. S2 in the SI). The C_2H_6 TPRS feature at 150-185 K is consistent with the desorption of relatively strongly-bound C_2H_6 σ-complexes adsorbed on the Ir_{cus} atoms of $IrO_2(110)$. Using Redhead analysis with a maximum value of the desorption pre-factor (5.9×10^{17} s^{-1}), we predict a binding energy of 65 kJ/mol for the C_2H_6 TPRS peak at 185 K. We also estimate a saturation coverage of ~0.30 ML for C_2H_6 σ-complexes on $IrO_2(110)$, based on the amount of C_2H_6 that desorbs above ~135 K plus the total amount that reacts. Our estimate agrees to within about 20% of the saturation coverage of C_2H_6 σ-complexes on $RuO_2(110)$.[18] Because the σ-complexes serve as dissociation precursors (see below), our TPRS results reveal that C_2H_6 C-H bond cleavage occurs readily on $IrO_2(110)$ at temperatures between ~150 and 200 K, i.e., in the same range as desorption of the C_2H_6 σ-complexes. We are unaware of other materials that exhibit such high activity toward promoting the C-H bond activation of C_2H_6.

We have recently shown that $IrO_2(110)$ is exceptionally active in promoting CH_4 C-H bond cleavage at temperatures as low as 150 K.[10] The present results demonstrate a similarly high reactivity of $IrO_2(110)$ toward C_2H_6 activation. Our prior study shows that CH_4 initially adsorbs on Ir_{cus} atoms and undergoes C-H bond cleavage by a heterolytic pathway involving H-atom transfer to a neighboring O_{br} atom, producing CH_3-Ir_{cus} and HO_{br} groups. We found that the energy barrier for CH_4 bond cleavage is nearly 10 kJ/mol lower than the binding energy of the CH_4 σ-complex, resulting in near unit dissociation probability for CH_4 on $IrO_2(110)$ at low

temperature and coverage. The resulting CH_3 groups are oxidized by the surface to CO, CO_2 and H_2O that desorb in TPRS features that are similar to those observed in the present study for C_2H_6 oxidation on $IrO_2(110)$. This similarity suggests that common reaction steps control the rates of CO, CO_2 and H_2O production during the oxidation of CH_4 and C_2H_6 on $IrO_2(110)$, after initial C-H bond cleavage. We previously reported that CH_4 oxidation to CO, CO_2 and H_2O is favored at low CH_4 coverage, but that recombinative desorption of CH_4 competes with oxidation at higher initial CH_4 coverage.[10] Our current results demonstrate that C_2H_6 also preferentially oxidizes during TPRS when the initial C_2H_6 coverage is sufficiently low. A key difference is that C_2H_6 dehydrogenates to C_2H_4 on $IrO_2(110)$ at high initial C_2H_6 coverage rather than recombinatively desorbing, and generates C_2H_4 at relatively low temperature (~300 to 450 K).

We show below that the coverage of HO_{br} groups plays a decisive role in determining the branching between C_2H_6 oxidation and C_2H_4 production. The proposed steps for C_2H_6 activation and subsequent dehydrogenation on $IrO_2(110)$ are the following,

Initial C_2H_6 dissociation vs. desorption: $C_2H_6(ad) \rightarrow C_2H_6(g)$

$C_2H_6(ad) + O_{br} \rightarrow C_2H_5(ad) + HO_{br}$

C_2H_5 dehydrogenation: $C_2H_5(ad) + O_{br} \rightarrow C_2H_4(ad) + HO_{br}$

C_2H_4 dehydrogenation vs. desorption: $C_2H_4(ad) + O_{br} \rightarrow C_2H_3(ad) + HO_{br}$

$C_2H_4(ad) \rightarrow C_2H_4(g)$

Ethane initially adsorbs in a molecular state $C_2H_6(ad)$ and forms a σ-complex by datively bonding with Ir_{cus} atoms, and a competition between dissociation and desorption of the $C_2H_6(ad)$ species determines the net probability of initial C-H bond cleavage. Our TPRS results show that

dissociation of the C_2H_6(ad) species is strongly favored over desorption at low C_2H_6 coverages. Since dissociation of the C_2H_6(ad) species requires an O_{br} atom, a decrease in the coverage of O_{br} atoms via conversion to HO_{br} groups may be mainly responsible for C_2H_6 dissociation reaching saturation during TPRS beyond a critical C_2H_6 coverage. After initial dissociation, the resulting C_2H_5(ad) species can dehydrogenate to C_2H_4(ad) species, and the C_2H_4(ad) species can either desorb or further dehydrogenate via H-atom transfer to an O_{br} atom. Again, the coverage of O_{br} atoms decreases with increasing C_2H_6 coverage because an increasing fraction of the O_{br} atoms is converted to HO_{br} groups via dehydrogenation of the C_2H_6-derived species. According to the proposed reaction steps, C_2H_4 desorption should become favored as the O_{br} atom coverage decreases.

Product yields as a function of the C_2H_6 coverage

Figure 2 shows the initial and reacted TPRS yields of C_2H_6 σ-complexes as a function of the initial C_2H_6 coverage on IrO_2(110) as well as the yields of C_2H_6 that converts to C_2H_4 vs. oxidizing to CO_x species. We set the total reacted yield of C_2H_6 equal to the sum of the C_2H_4 yield plus one half of the yield of CO + CO_2, where the factor of one half converts the CO_x yield to the amount of C_2H_6 that oxidizes, and we define the initial amount of C_2H_6 σ-complexes as equal to the reacted C_2H_6 yield plus the amount of C_2H_6 that desorbs in the TPRS feature above ~135 K. Our results show that 90 to 100% of the strongly-bound C_2H_6 reacts during TPRS as the C_2H_6 coverage increases to ~0.25 ML, at which point the yield of reacted C_2H_6 begins to plateau toward a value of 0.20 ML and the yield of C_2H_6 σ-complexes that desorb concurrently increases. The reacted C_2H_6 yield corresponds to about 67% of the adsorbed C_2H_6 complexes at saturation. Our results demonstrate that a large quantity of C_2H_6 reacts on IrO_2(110) during

TPRS, and thus support the conclusion that initial C-H activation and subsequent reaction occur on the crystalline terraces of $IrO_2(110)$.

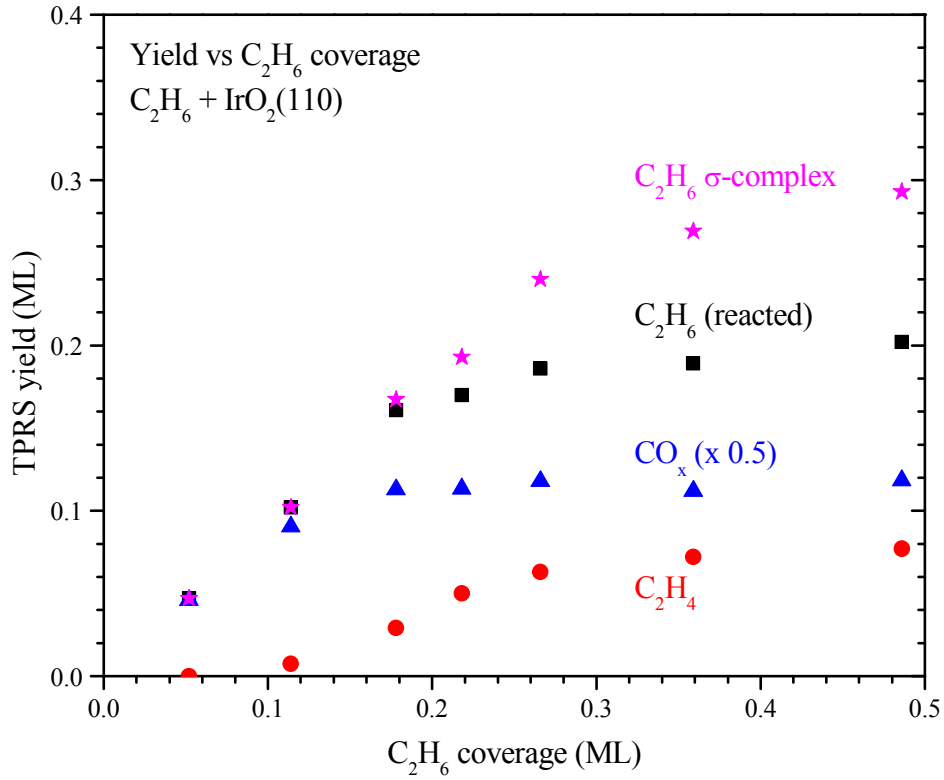

Figure 2: TPRS product yields as a function of the initial coverage of C_2H_6 adsorbed on $IrO_2(110)$ at 90 K, including the initial coverage of C_2H_6 σ-complexes (desorbed + reacted), the reacted yield of C_2H_6, the C_2H_4 yield and the yield of ethane that oxidizes ($0.5*CO_x$).

Our results further show that C_2H_6 oxidation is strongly favored at low coverage, and that C_2H_4 production initiates at moderate coverage as the CO_x yield begins to saturate. The yield of oxidized ethane increases nearly to saturation with increasing C_2H_6 coverage to about 0.15 ML, and thereafter plateaus at a value of about 0.12 ML. Ethylene production first becomes evident at a C_2H_6 coverage above 0.10 ML and increases toward a plateau value as the total C_2H_6 coverage

rises to ~0.30 ML. The maximum C_2H_4 yield is equal to 0.08 ML at saturation of the C_2H_6 σ-complexes, and represents a large fraction (~38%) of the C_2H_6 that reacts on $IrO_2(110)$. The evolution of the product yields with the C_2H_6 coverage suggests that the availability of O_{br} atoms plays a decisive role in determining the reaction pathways that adsorbed C_2H_6 molecules can access on $IrO_2(110)$. Notably, our current results show that the CO_x yield saturates at an O_{br}:C_2H_6 ratio close to five; however, the actual minimum O_{br}:C_2H_6 ratio needed to promote C_2H_6 oxidation to CO_x may be less than five because background H_2 adsorption converts ~0.15 to 0.25 ML of the initial O_{br} atoms to HO_{br} groups prior to the C_2H_6 TPRS experiment.

Enhanced selectivity for C_2H_4 production on H-covered $IrO_2(110)$

We find that the selectivity toward C_2H_4 production from C_2H_6 can be enhanced by pre-hydrogenating the $IrO_2(110)$ surface. Figure 3a compares TPRS traces of the 27 and 44 amu fragments obtained after adsorbing ~0.14 ML of C_2H_6 on clean $IrO_2(110)$ vs. an $IrO_2(110)$ surface with an estimated H-atom pre-coverage of 0.32 ML. The 27 amu TPRS trace exhibits well-separated features arising from C_2H_6 and C_2H_4, and the 44 amu feature alone is sufficient for representing the change in CO_x production because surface hydrogenation causes similar changes in the CO and CO_2 TPRS features.

Our results show that pre-hydrogenating the surface to a moderate extent (<~0.4 ML) causes the CO_2 TPRS peak to diminish, while the C_2H_4 TPRS feature intensifies and skews toward lower temperature, with the maximum shifting from 445 to 350 K. Pre-hydrogenation also causes a C_2H_6 TPRS peak at ~175 K to gain intensity, whereas this peak is negligible after generating a moderate C_2H_6 coverage on clean $IrO_2(110)$ (SI). These changes show that pre-hydrogenating $IrO_2(110)$ suppresses C_2H_6 oxidation to CO_x species but enhances C_2H_4

production when the H-atom pre-coverage is moderate. The concurrent increase in the C_2H_6 TPRS peak at 175 K correlates with the decrease in CO_x TPRS yields, and thus demonstrates that surface pre-hydrogenation causes a fraction of the adsorbed C_2H_6 σ-complexes to desorb rather than oxidize. This behavior provides further evidence that adsorbed C_2H_6 σ-complexes serve as precursors to reaction and that dissociation involves H-atom transfer to O_{br} atoms.

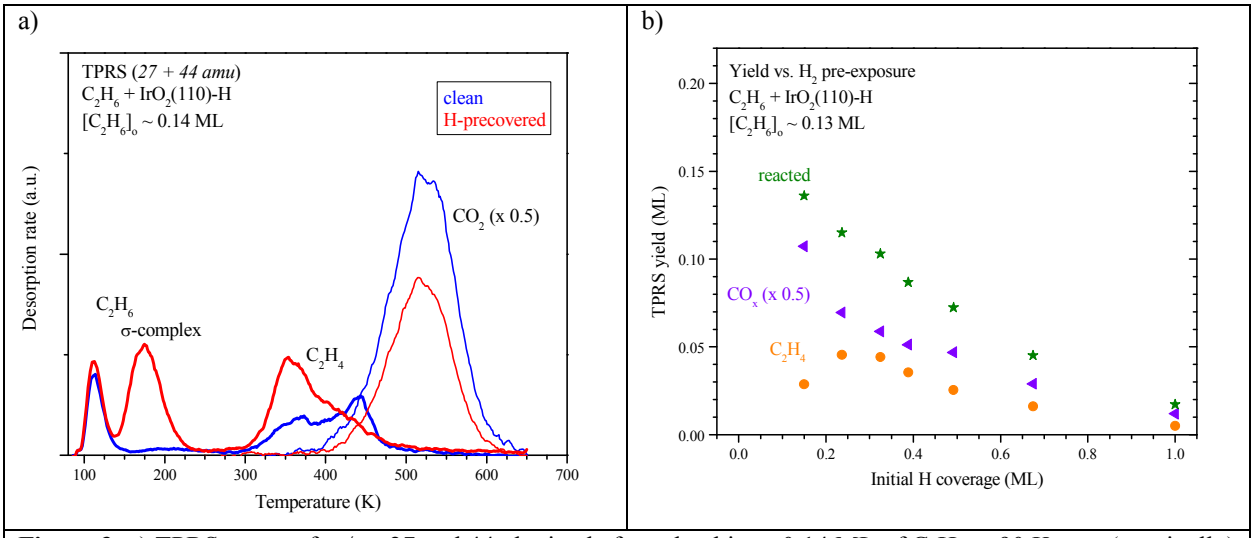

Figure 3: a) TPRS traces of *m/z* = 27 and 44 obtained after adsorbing ~0.14 ML of C_2H_6 at 90 K on a (nominally) clean $IrO_2(110)$ surface (blue) and an $IrO_2(110)$ surface with a hydrogen pre-coverage of 0.32 ML (red). The 27 and 44 amu traces are represented by thick vs. thin lines. b) Total reacted C_2H_6 yield, oxidized C_2H_6 yield ($0.5*CO_x$) and C_2H_4 yield obtained as a function of the hydrogen pre-coverage during TPRS for a C_2H_6 coverage of ~0.13 ML.

Figure 3b shows how the total TPRS yield of reacted C_2H_6 as well as the yields of the C_2H_4 and CO_x reaction products evolve as a function of the initial H-atom coverage on $IrO_2(110)$, for an initial C_2H_6 coverage of 0.13 ± 0.015 ML. We estimate that the nominally clean $IrO_2(110)$ surface was covered by ~0.15 ML of H-atoms prior to ethane adsorption. Our results show that the total yield of reacted C_2H_6 decreases monotonically with increasing H-atom pre-coverage, indicating that initially converting O_{br} atoms to HO_{br} groups suppresses C_2H_6 activation on $IrO_2(110)$. The CO_x yield decreases sharply and continuously from a value of 0.11 to 0.01 ML as

the H-atom coverage increases to about 1 ML. In contrast, however, the C_2H_4 yield increases from ~0.03 to 0.045 ML with increasing H-atom coverage to ~0.32 ML and thereafter decreases, reaching a final value of 0.005 ML at saturation of the initial H-atom layer. The C_2H_4 yield begins to fall below its value on the (nominally) clean $IrO_2(110)$ surface when the initial H-atom coverage starts to exceed 0.5 ML. These changes represent a nearly threefold increase in the selectivity for C_2H_4 production, as measured by the ratio of ethane that converts to ethylene vs CO_x species, i.e., selectivity equals $2[C_2H_4]/[CO_x]$. The selectivity increases to 0.75 at moderate C_2H_6 coverage (~0.13 ML) and hydrogen pre-coverage, and is thus slightly higher than the selectivity of 0.65 achieved at high C_2H_6 coverage on nominally clean $IrO_2(110)$. It may be possible to achieve even higher selectivity for C_2H_4 production by performing experiments at high C_2H_6 coverage on partially-hydrogenated $IrO_2(110)$. The evolution of product yields with increasing H-coverage demonstrates that O_{br} atoms are needed to promote the initial C-H activation of C_2H_6 on $IrO_2(110)$ as well as further dehydrogenation and that the controlled deactivation of O_{br} atoms by hydrogenation provides a means to enhance reaction selectivity to favor the conversion of ethane to ethylene.

Pathways for C_2H_6 dehydrogenation on $IrO_2(110)$

We examined several possible C_2H_6 adsorption configurations (see Fig. S4 in SI) and predict that C_2H_6 forms a strongly-bound σ-complex on $IrO_2(110)$ by adopting a flat-lying geometry along the Ir_{cus} row in which each CH_3 group forms a H-Ir_{cus} dative bond (a $2\eta^1$ configuration) and the C_2H_6 molecule effectively occupies two Ir_{cus} sites. This staggered $2\eta^1$ configuration is similar to that predicted by Pham et al. but they report an eclipsed C_2H_6 $2\eta^1$ configuration,[22] which we find

to be less stable than the staggered configuration by ~9 kJ/mol (Fig. S4). We have previously reported that C_2H_6 complexes on PdO(101) and RuO_2(110) also preferentially adopt the $2\eta^1$ configuration.[18,23,24]

Figure 4a shows the energy diagram computed using DFT-D3 for the sequential dehydrogenation of C_2H_6 to C_2H_4 on IrO_2(110), followed by either C_2H_4 desorption (red) or C_2H_4 dehydrogenation to adsorbed C_2H_3. DFT-D3 predicts that the $2\eta^1$ C_2H_6 complex achieves a binding energy of 107 kJ/mol on clean IrO_2(110) and that the barrier for C-H bond cleavage via H-transfer to an O_{br} atom is only 38 kJ/mol. According to the calculations C_2H_6 dehydrogenation to produce C_2H_5-Ir_{cus} and HO_{br} species is exothermic by about 97 kJ/mol, and the barrier for reaction is significantly lower than the binding energy of the adsorbed C_2H_6 complex (38 vs. 107 kJ/mol). We find that DFT-PBE calculations without dispersion corrections underestimate the C_2H_6 binding energy on IrO_2(110), but still predict that the C_2H_6 dissociation barrier is lower than the desorption barrier (Table S1). Our calculations thus predict that C_2H_6 C-H bond cleavage is strongly favored over molecular desorption on clean IrO_2(110) such that all adsorbed C_2H_6 molecules will dissociate at low temperature, provided that O_{br} atoms are available for reaction. This prediction agrees well with our experimental finding that C_2H_6 dissociates on IrO_2(110) with near unit probability at low C_2H_6 coverages (Figure 2).

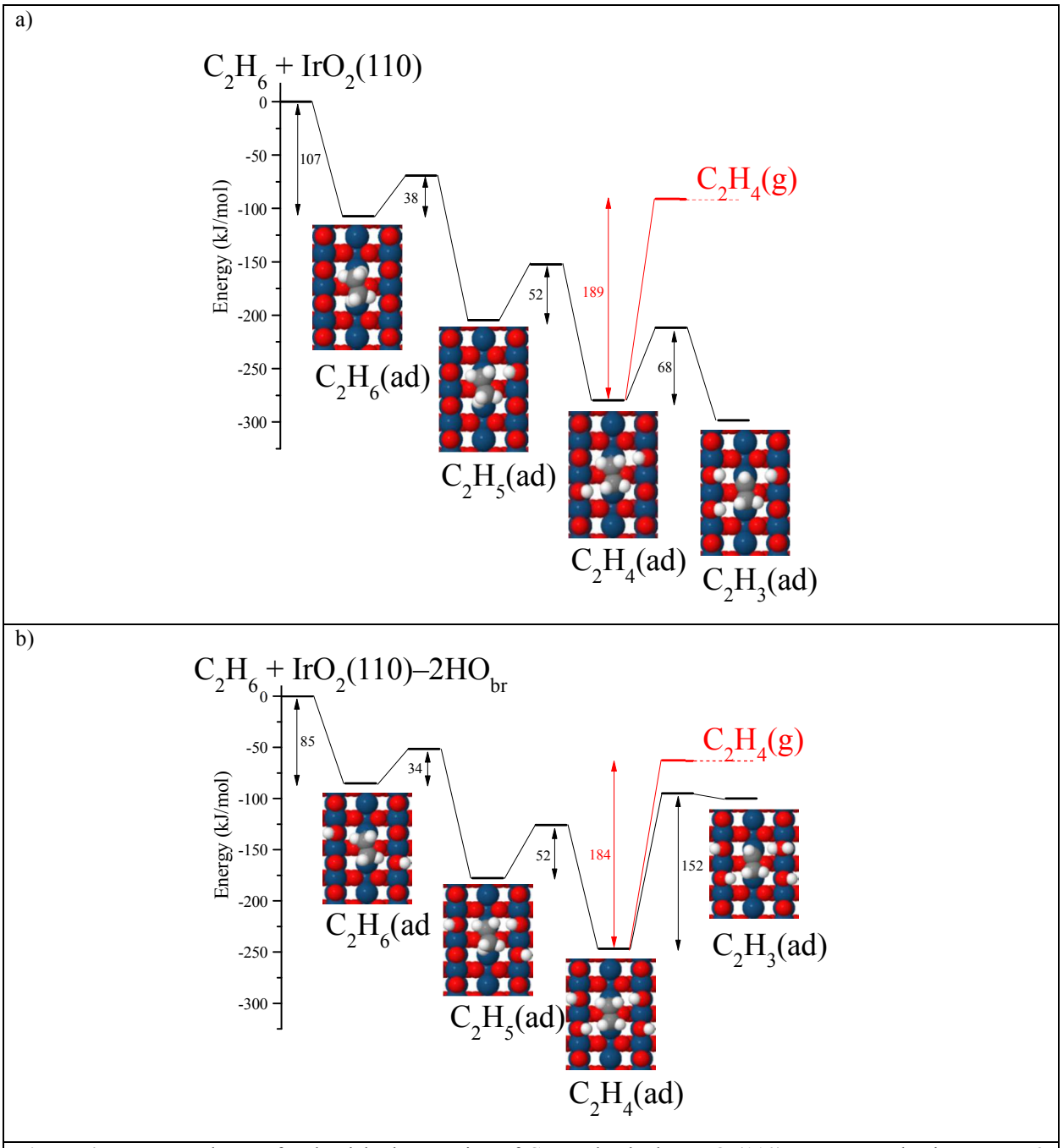

Figure 4: Energy pathways for the dehydrogenation of C_2H_6 adsorbed on $IrO_2(110)$ as computed using DFT-D3 for surfaces initially containing (a) zero and (b) two HO_{br} groups. The final reaction step compares the energy changes for C_2H_4 desorption (red) vs. dehydrogenation to a C_2H_3(ad) species (black). A comparison of the energetics for these pathways with and without D3 can be found in Table S1 in the SI.

We find that the adsorbed C_2H_5 group on $IrO_2(110)$ can also dehydrogenate by a low energy pathway wherein the CH_3 group transfers a H-atom to an O_{br} atom, resulting in an adsorbed C_2H_4

species and a HO_{br} group located in the opposing row from the initial HO_{br} group (Figure 4a). DFT-D3 predicts an energy barrier of 52 kJ/mol for this reaction and an exothermicity of 75 kJ/mol. The barrier for C_2H_5 dehydrogenation is relatively low because the CH_3 group maintains a H-Ir_{cus} dative interaction that weakens one of the C-H bonds. The C_2H_4 product adopts a bidentate geometry in which a C-Ir_{cus} σ-bond forms at each CH_2 group (i.e., di-σ configuration). Our calculations predict that the C_2H_4 species needs to overcome a barrier of 189 kJ/mol to desorb vs. a barrier of 68 kJ/mol to dehydrogenate via H-transfer to an O_{br} atom, affording an adsorbed C_2H_3 species and a third HO_{br} group. The calculations thus predict that C_2H_4 dehydrogenation is strongly favored over C_2H_4 desorption when O_{br} atoms are available to serve as H-atom acceptors. This prediction is consistent with our experimental observation that C_2H_6 oxidation occurs preferentially over C_2H_4 production at low initial C_2H_6 and HO_{br} coverages.

Figure 4b shows the computed pathway for C_2H_6 dehydrogenation on $IrO_2(110)$ when two of the four accessible O_{br} atoms are initially hydrogenated to HO_{br} groups. For these calculations, we hydrogenated O_{br} atoms located in opposing rows, with each next to a different CH_3 group of the C_2H_6 complex (Figure 4b). Our calculations predict that hydrogenation of the two O_{br} atoms destabilizes the C_2H_6 σ-complex on $IrO_2(110)$ by about 22 kJ/mol. We have recently reported that the hydrogenation of O_{br} atoms also destabilizes H_2 complexes on $IrO_2(110)$.[11] Our calculations also predict that the energy barriers are nearly the same for C_2H_6 and C_2H_5 dehydrogenation on the initially clean $IrO_2(110)$ vs. pre-hydrogenated $IrO_2(110)$-$2HO_{br}$ surfaces when reaction occurs by H-transfer to an O_{br} atom (Figures 4a, b).

Sequential dehydrogenation of C_2H_6 to C_2H_4 on the initial $IrO_2(110)$-$2HO_{br}$ surface converts all four of the accessible O_{br} atoms to HO_{br} groups, and causes C_2H_4 desorption to become favored over further dehydrogenation because HO_{br} groups are much less reactive than O_{br}

atoms. The energy barrier for C_2H_4 dehydrogenation via H-transfer to a HO_{br} group is 152 kJ/mol, compared with 68 kJ/mol for C_2H_4 dehydrogenation to an O_{br} atom. In addition, the reverse reaction features an energy barrier of only 5 kJ/mol so the H_2O_{br} species would rapidly transfer a H-atom to C_2H_3 to regenerate the adsorbed C_2H_4 and HO_{br} species. Our DFT calculations thus indicate that C_2H_4 desorption is favored over dehydrogenation when all of the accessible O_{br} atoms are hydrogenated to HO_{br}. This prediction agrees well with our experimental findings that pre-hydrogenation of $IrO_2(110)$ promotes the conversion of C_2H_6 to C_2H_4 while suppressing C_2H_6 oxidation, and that C_2H_4 production begins to occur on initially clean $IrO_2(110)$ only at moderate initial C_2H_6 coverages.

Discussion

Our results show that C_2H_6 activation is highly facile on $IrO_2(110)$ at temperatures below 200 K, and that further dehydrogenation produces C_2H_4 that desorbs between 300 and 450 K. Based on comparison with reference TPRS data (SI), we conclude that C_2H_4 desorption is the rate-limiting step in the conversion of C_2H_6 to C_2H_4 on $IrO_2(110)$ during TPRS. Our DFT calculations support these conclusions as they predict that the barrier for C_2H_6 C-H bond cleavage on clean $IrO_2(110)$ is lower than that for C_2H_4 desorption by at least 100 kJ/mol. Indeed, we find that the $IrO_2(110)$ surface is exceptionally active in promoting alkane C-H bond cleavage - we estimate a barrier between 35 and 40 kJ/mol for ethane activation on $IrO_2(110)$, and our prior work reveals an even lower barrier of 28 kJ/mol for CH_4 activation on $IrO_2(110)$.[10] In fact, our DFT results predict that initial C-H bond cleavage has the lowest barrier among the reaction steps involved in C_2H_6 conversion to C_2H_4 on $IrO_2(110)$.

In contrast to $IrO_2(110)$, initial C-H bond activation is the rate-determining step in the ODH of alkanes on most other oxides. Supported vanadium-oxide based catalysts have been widely studied due to their favorable performance in promoting the ODH of ethane and propane.[1,9] While the specific values can depend on multiple factors, barriers for ethane C-H bond cleavage on VO_x-based catalysts lie in a range from about 120 to 150 kJ/mol,[5,25,26] and reactors are operated at temperatures between 700 and 900 K to achieve optimal rates and selectivity of alkene production from ethane and propane.[2] According to DFT, ethylene desorption is the rate-determining step for the conversion of C_2H_6 to C_2H_4 on $IrO_2(110)$ under TPRS conditions because the dehydrogenation of adsorbed C_2H_6 and C_2H_5 groups are both facile processes on clean $IrO_2(110)$ and the C_2H_4 product binds strongly. From our TPRS data, we estimate that the barrier for C_2H_4 desorption from $IrO_2(110)$ lies between about 130 and 165 kJ/mol, and is thus close to the values reported for C_2H_6 C-H activation barriers on VO_x-based catalysts. However, since the entropy of activation is much larger for C_2H_4 desorption compared with ethane C-H bond cleavage, C_2H_4 desorbs from $IrO_2(110)$ at lower temperature relative to the temperatures at which VO_x-based catalysts would achieve comparable rates of ethane conversion to ethylene.

Our TPRS results show that the desorption of ethylene from $IrO_2(110)$ occurs at lower temperature during TPRS than the reaction-limited desorption of H_2O and CO_x species resulting from ethane oxidation (Figure 1). A possible implication is that low temperature operation can enable IrO_2 catalysts to promote the conversion of ethane to ethylene at high rates while minimizing CO_x production. However, the higher desorption temperature of H_2O compared with C_2H_4 suggests that H_2O desorption could be a rate-controlling step in the IrO_2-promoted conversion of C_2H_6 to C_2H_4 under steady-state conditions. While further study is needed, our

results suggest possibilities for achieving efficient and selective conversion of ethane to ethylene at low temperature using IrO_2-based catalysts.

Our results also demonstrate that partial hydrogenation of the $IrO_2(110)$ surface enhances ethane conversion to ethylene while suppressing extensive oxidation to CO_x species. We find that HO_{br} groups are significantly less active than O_{br} atoms as H-atom acceptors, and, as a result, hydrogenating a fraction of the O_{br} atoms limits the extent to which adsorbed hydrocarbons can dehydrogenate and causes C_2H_4 desorption to become favored over further dehydrogenation and extensive oxidation. This behavior provides a viable explanation of the evolution of TPRS product yields with increasing C_2H_6 coverage. At low C_2H_6 coverage enough O_{br} atoms are available to allow each C_2H_6 molecule to extensively dehydrogenate, and produce intermediates that oxidize to CO_x species with further heating. With increasing C_2H_6 coverage, the extent to which C_2H_6 molecules dehydrogenate becomes limited because a larger fraction of O_{br} atoms convert to HO_{br} groups and deactivate. Consistent with this interpretation, our experiments demonstrate that the selectivity toward ethane conversion to ethylene can be enhanced by partially hydrogenating the $IrO_2(110)$ surface prior to adsorbing ethane. This finding may have broad implications for developing methods by which to modify the selectivity of IrO_2 catalysts. In particular, our results demonstrate that controllably deactivating a fraction of the reactive O-atoms of IrO_2 is an effective approach for promoting the partial dehydrogenation of ethane over extensive oxidation.

Summary

We investigated the dehydrogenation of ethane on the stoichiometric $IrO_2(110)$ surface using TPRS and DFT calculations. Our results show that ethane forms strongly-bound σ-complexes on $IrO_2(110)$ and that a large fraction of the adsorbed complexes undergo C-H bond cleavage below 200 K during TPRS. Our DFT calculations predict that ethane σ-complexes on $IrO_2(110)$ dissociate by a heterolytic mechanism involving H-atom transfer to a neighboring O_{br} atom, and that the barrier for C-H bond cleavage is lower than the binding energy of the C_2H_6 σ-complex. We find that the resulting ethyl groups react with the $IrO_2(110)$ surface via oxidation to CO_x species and H_2O as well as dehydrogenation to C_2H_4, with the C_2H_4 product desorbing between 300 and 450 K. Both DFT calculations and TPRS experiments show that C_2H_4 desorption is the rate-limiting step in the conversion of C_2H_6 to C_2H_4 on $IrO_2(110)$ during TPRS. Our experimental results demonstrate that partially hydrogenating the $IrO_2(110)$ surface enhances the conversion of ethane to ethylene while suppressing ethane oxidation to CO_x species. According to DFT, converting a fraction of the O_{br} atoms to HO_{br} groups causes C_2H_4 desorption to become favored over further dehydrogenation because HO_{br} groups are poor H-atom acceptors compared to O_{br} atoms. Our findings reveal that the $IrO_2(110)$ surface exhibits an unusual ability to promote the dehydrogenation of ethane to ethylene near room temperature during TPRS, and demonstrate that controlled deactivation of O_{br} atoms is an effective way to promote ethylene production from ethane on $IrO_2(110)$.

Supporting Information

Structural representation of the $IrO_2(110)$ surface; Measurement of product yields; TPRS traces for C_2H_6 as a function of coverage on $IrO_2(110)$; TPRS traces for C_2H_4 adsorbed on $IrO_2(110)$ at 90 K; Configurations of C_2H_6 adsorbed on $IrO_2(110)$ as predicted with DFT; Comparison of

DFT-PBE calculations with and without dispersion-corrections for C_2H_6 dehydrogenation on $IrO_2(110)$. This material is available free of charge via the Internet at http://pubs.acs.org.

Acknowledgements

We acknowledge the Ohio Supercomputing Center for providing computational resources. We gratefully acknowledge financial support for this work provided by the Department of Energy, Office of Basic Energy Sciences, Catalysis Science Division through Grant DE-FG02-03ER15478.

References

(1) Gartner, C. A.; van Veen, A. C.; Lercher, J. A. *Chemcatchem* **2013**, *5*, 3196.
(2) Cavani, F.; Ballarini, N.; Cericola, A. *Catal. Today* **2007**, *127*, 113.
(3) Banares, M. A. *Catal. Today* **1999**, *51*, 319.
(4) Gartner, C. A.; van Veen, A. C.; Lercher, J. A. *J. Am. Chem. Soc.* **2014**, *136*, 12691.
(5) Argyle, M. D.; Chen, K. D.; Bell, A. T.; Iglesia, E. *J. Catal.* **2002**, *208*, 139.
(6) Argyle, M. D.; Chen, K. D.; Bell, A. T.; Iglesia, E. *J. Phys. Chem. B* **2002**, *106*, 5421.
(7) Martinez-Huerta, M. V.; Gao, X.; Tian, H.; Wachs, I. E.; Fierro, J. L. G.; Banares, M. A. *Catal. Today* **2006**, *118*, 279.
(8) Rozanska, X.; Fortrie, R.; Sauer, J. *J. Am. Chem. Soc.* **2014**, *136*, 7751.
(9) Carrero, C. A.; Schloegl, R.; Wachs, I. E.; Schomaecker, R. *ACS Catal* **2014**, *4*, 3357.
(10) Liang, Z.; Li, T.; Kim, M.; Asthagiri, A.; Weaver, J. F. *Science* **2017**, *356*, 298.
(11) Li, T.; Kim, M.; Liang, Z.; Asthagiri, A.; Weaver, J. F. *Top. Catal.* **2017**, DOI: 10.1007/s11244.
(12) Blochl, P. E. *Phys. Rev. B* **1994**, *50*, 17953.
(13) Kresse, G. *J. Non-Cryst. Solids* **1995**, *193*, 222.
(14) Kresse, G.; Hafner, J. *J. Non-Cryst. Solids* **1993**, *156*, 956.
(15) Perdew, J. P.; Burke, K.; Ernzerhof, M. *Phys. Rev. Lett.* **1996**, *77*, 3865.
(16) Grimme, S.; Antony, J.; Ehrlich, S.; Krieg, H. *J. Chem. Phys.* **2010**, *132*, 154104.
(17) Weaver, J. F.; Hakanoglu, C.; Antony, A.; Asthagiri, A. *Chem. Soc. Rev.* **2014**, *43*, 7536.
(18) Li, T.; Kim, M.; Rai, R.; Liang, Z.; Asthagiri, A.; Weaver, J. F. *Phys. Chem. Chem. Phys.* **2016**, *18*, 22647.
(19) Henkelman, G.; Uberuaga, B. P.; Jonsson, H. *J. Chem. Phys.* **2000**, *113*, 9901.
(20) Chen, L.; Smith, R. S.; Kay, B. D.; Dohnalek, Z. *Surf. Sci.* **2016**, *650*, 83.
(21) Tait, S. L.; Dohnalek, Z.; Campbell, C. T.; Kay, B. D. *J. Chem. Phys.* **2006**, *125*, 234308.
(22) Pham, T. L. M.; Nachimuthu, S.; Kuo, J. L.; Jiang, J. C. *Appl. Catal., A* **2017**, *541*, 8.
(23) Antony, A.; Asthagiri, A.; Weaver, J. F. *J. Chem. Phys.* **2013**, *139*, 104702: 1.
(24) Antony, A.; Hakanoglu, C.; Asthagiri, A.; Weaver, J. F. *J. Chem. Phys.* **2012**, *136*, 054702.
(25) Dai, G. L.; Liu, Z. P.; Wang, W. N.; Lu, J.; Fan, K. N. *J. Phys. Chem. C* **2008**, *112*, 3719.
(26) Cheng, M. J.; Goddard, W. A. *J. Am. Chem. Soc.* **2015**, *137*, 13224.

ToC Graphic